

---

## Katian volcanism in Central Armorican Domain (France) and Central Iberian Zone (Portugal): a single monogenetic basaltic field?

Caroff Martial <sup>1,\*</sup>

<sup>1</sup> UMR/CNRS n°6538, Laboratoire Géo-Océan CNRS/IFREMER/UBO/UBS, Université de Brest, Institut Universitaire Européen de la Mer, Place Nicolas Copernic, 29280 Plouzané, France

\* Corresponding author : Martial Caroff, email address : [caroff@univ-brest.fr](mailto:caroff@univ-brest.fr)

---

### Abstract :

The Crozon peninsula and Buçaco syncline belong respectively to the Central Armorican Domain (CAD) and the Central Iberian Zone (CIZ), located on both sides of the Variscan “Ibero-Armorican Arc” structure at present. The Ordovician sedimentary successions in both sites are known to display identical lithofacies. The paired Upper Katian formations also exhibit comparable volcanic successions of anorogenic affinity, including volcanoclastic beds and pillow lavas. The tephra deposits are inferred to have resulted from the activity of subaqueous monogenetic basaltic tuff cones above a < 100 m-deep calcareous soft-substrate, in context of passive margin. The Surtseyan-style hydrovolcanic eruptions were followed by effusion of pillow lavas. Both sites also display a large range of similar peperite facies, sometimes related to magmatic segregation structures likely to derive from vapor-differentiation. The deeper doleritic dykes and sills, comparable in terms of mineralogy and geochemistry, contain identical metasedimentary xenoliths, whose high temperature phyllosilicates display a very restricted range of compositions. In the Late Ordovician, Crozon and Buçaco were probably nearby volcanic edifices belonging to a single monogenetic field inside the Armorica microplate. The sudden appearance of high-latitude Katian carbonates, associated with volcanism only in these two peri-Gondwanan sites, has just preceded the Gondwanan Hirnantian glaciation.



## **Supplementary Material**

Table S1; Table S2; Table S3; Fig. S1.

Early Paleozoic rift-related magmatism has been recorded in various southern domains of the Variscan Europe, such as the Alpine basement, the Maures Massif, the Corsica and Sardinia islands (see Crowley *et al.* 2000 and references therein), and the Armorican Massif (Caroff *et al.* 2009; this study). These magmatic episodes were linked to a large fragmentation event of the northern Gondwana margin, resulting in the formation of terrane assemblages separated by marine areas (Crowley *et al.* 2000). The ATA (Armorican Terrane Assemblage), also known as Armorican microplate (Matte 2001; Fernández-Suárez *et al.* 2002; Robardet 2003), was one of these continental archipelagoes, comprising a Gondwana-derived Cadomian block in its northern part (Le Gall *et al.* 2021). Despite the fact that the Ordovician paleogeography is nowadays relatively well constrained on a global scale, especially since the works of Fortey and Cocks (2003), Franke *et al.* (2017) and Cocks and Torsvik (2021), the regional features of such terrane assemblages (including domain arrangement, geoenvironment, sedimentary and volcanic features), are still little known.

Since the pioneering studies of Henry *et al.* (1974, 1976), Paris and Robardet (1977), Robardet *et al.* (1990), and Robardet and Gutierrez Marco (1990), we know that the stratigraphic succession in the Central Armorican Domain (CAD, Armorican Massif) was very similar to that in the Central Iberian Zone (CIZ, Iberian Massif) during the Ordovician times, as demonstrated by sedimentary and paleontological data. Indeed, both Ordovician successions in Crozon peninsula (CAD) and Buçaco syncline (CIZ) show identical lithofacies and benthic assemblages.

The study of the Upper Katian volcanism from Crozon (France) by Caroff *et al.* (2009) revealed that the corresponding volcanic edifice was a subaqueous basaltic tuff cone emplaced in a calcareous soft-substrate environment at the top of a siliciclastic succession, in context of passive margin. This episode is part of a global Katian volcanic event which predated the Hirnantian glaciation (Lefebvre *et al.* 2010; Bond and Grasby 2020; Hu *et al.*

2021). As comparable hypabyssal intrusives, volcanoclastics and associated peperites are observable in coeval and analogous formations in the Buçaco syncline (Portugal) (Young 1988; Colmenar *et al.* 2017a, b; 2019), a detailed comparison between the volcanic facies from both areas appears to be required, by taking into account new geological, paleovolcanological, mineralogical and geochemical data, aimed at refining the paleogeographic reconstructions and discussing the relative position of CAD and CIZ inside the Armorica microplate in the Late Ordovician.

## Geology

### *Comparative stratigraphy*

The Crozon peninsula (France) shows a noteworthy sedimentary succession continuously cropping out along the foreshore and cliffs from the Cambrian to the Upper Devonian (Vidal *et al.* 2011). It is composed of two structural units, the South unit being overthrust by the North one (Caroff *et al.* 2009; Fig. 1a, b). Both units recorded the same geological events, except at the base of the sedimentary pile (lack of Floian Red Sandstone Formation and thinner Floian Armorican Sandstone Formation in the North unit) and at its top (lack of Upper Katian volcanics and limestones in the North unit) (Fig. 2). From the Middle to the Upper Ordovician, the South Crozon succession includes many hypabyssal rocks, mainly lobate dykes and sills (globular peperites) in the Dapingian/Darriwilian/Sandbian siliciclastic Postolonnec Formation (Kerdreux site: Fig. 1b) and in the Katian siliciclastic Kermeur / tuffaceous Rosan Formations (Trégarvan, Kerdra, and Aber sites: Fig. 1a, b) (Figs 2 and 3a, c). In the North Crozon unit, we observe only a few narrow peperitic dykes in the Postolonnec beach (Fig. 1b). All these intrusive sheets have been interpreted by Caroff *et al.* (2009) as

subvolcanic bodies having fed one or several Upper Katian subaqueous volcano(es), at the origin of the volcanoclastics and lavas characteristic of the Rosan formation (Fig. 2). The corresponding facies consist of tuffaceous deposits (in silicified and decalcified limestone, Aber site; Fig. 3e, f), pillow lavas (in decalcified limestone or limestone, Aber and Lostmarc'h sites; Caroff *et al.* 2009), and lobate clast-bearing rhythmic graded breccias (in limestone, Lostmarc'h site; Caroff *et al.* 2009). Volcanics and limestones of the Rosan Formation (South Crozon unit) are overlain by Hirnantian sandstones (Vidal *et al.* 2011), whereas, in the North Crozon unit, thicker Hirnantian glacio-marine diamictites exhibiting “ball and pillow” facies (Cosquer Formation) directly overlie an erosion level at the top of the Kermeur sandstones (Fig. 2).

In the Buçaco syncline (Portugal) (Fig. 1c, d), the stratigraphic succession is almost identical (Young 1988; Colmenar *et al.* 2017a, b; 2019). The only differences are: (1) the smaller thickness of the Katian Louredo Formation (equivalent to Kermeur); (2) lateral occurrence of Upper Katian volcanic rock-free argillaceous limestone/dolostone (Ferradosa Formation); and (3) occurrence of Hirnantian diamictites (Casal Carvalhal Formation, equivalent to the Cosquer Formation) above the Upper Katian volcanics (Porto de Santa Anna, equivalent to the Rosan Formation), and not laterally as in Crozon (Fig. 2). The Buçaco succession also comprises many peperitic hypabyssal rocks (Fig. 3b, d) in the Dapingian/Darriwilian/Sandbian siliciclastic Cécemes Group and in the Katian siliciclastic Louredo / tuffaceous Porto de Santa Anna Formations (Fig. 2). The volcanic Porto de Santa Anna Formation is mainly developed in the northern part of the Buçaco Syncline. It is composed of volcanoclastics with silicified matrix (Galhano site: Young 1988; Colmenar *et al.* 2017b; Fig. 3g) and pillow lavas (Cabeço Pedrogão site) (Fig. 1d).

### ***Volcanic successions***

In both localities, Crozon (France) and Buçaco (Portugal), there are two pairs of volcanic successions, each of them including similar facies: the first pair (Aber and Galhano, respectively) is predominantly clastic, whereas the other one (Lostmarc'h and Cabeço Pedrogão, respectively) is mostly effusive (Fig. 4).

The base of both Upper Katian Aber/Galhano successions is marked by a Fe-oolitic horizon (Fig. 4). They lie over the Lower-Middle Katian Kermeur/Louredo Formations. The two main breccia facies in the Aber site (Rosan Formation) correspond to volcanoclastic deposits. The first facies (facies C of Caroff *et al.* 2009) corresponds to crudely stratified polymict volcanoclastics, with decalcified matrix (Fig. 3e): poorly sorted beds (up to 2 m in thickness), normally or inversely graded; clast size < 5 cm; abundant sediment-derived chloritic fragments; silicic bioclastic matrix with volcanic shards and sediment-derived chloritic micro-fragments. These layers alternate with thin-bedded volcanoclastic layers (facies D of Caroff *et al.* 2009; Fig. 3f): well-sorted thin beds (from a few millimeters to a few centimeters in thickness); fluidal sediment-derived chloritic clasts and angular volcanic clasts in a mixed matrix composed of ash, chlorite and micro-bioclasts; there are two sub-facies (D1 and D2 of Caroff *et al.* 2009): (D1) ejecta < 1 cm in length (upper part of the photograph in Fig. 3f), and (D2) ejecta < 1 mm in length, planar matrix-poor beds and planar, wavy or convolute matrix-rich beds, with elongated parallel-aligned volcanic microclasts with the laminae and mm-sized load structures (lower part of the photograph in Fig. 3f). Both deposit types (C and D) are especially rich in chloritized clasts of sedimentary origin. This succession was intruded by fluidal peperitic sills or dykes (Fig. 4), sometimes disintegrated into amoeboid clasts (see below). At the top of the pile a few pillow lavas are interbedded with decalcified limestone strata just below a Hirnantian sandstone level (Fig. 4). The Galhano volcanoclastic succession (Porto de Santa Anna Formation) is less known, mainly due to

poorer outcrop conditions. It is also composed of volcanoclastic rocks (Fig. 3g), close to the Aber facies D shown in Fig. 3f, overlain by decalcified beds (Young 1988). The uppermost part of the formation is composed of a sequence of thinly-bedded fine-grained tuffaceous sediments and limestones cut by altered lobate hypabyssal intrusions (Young 1988; Colmenar *et al.* 2017b).

In both Lostmarc'h/Cabeço Pedrogão sites (Rosan/Porto de Santa Anna Formations), pillow lavas are largely dominant. The pile thickness is *c.* 10 m in Lostmarc'h (Paris *et al.* 1981) and *c.* 36 m in Cabeço Pedrogão (Fig. 4). The matrix is mainly calcareous in Lostmarc'h, including fossils and lava fragments, whereas it is principally composed of autoclastic volcanic breccias in Cabeço Pedrogão. Upon the Lostmarc'h pillow lavas and beneath a thick bioclastic limestone bed, an 8 m-thick lobate clast-bearing rhythmic fining-up graded breccia sequence crops out (Fig. 4). Such graded breccias lack in Cabeço Pedrogão, where the pillow lava pile is topped by fossiliferous marlstone layers (Fig. 4).

### **Peperites and other water-related structures**

The occurrence of fluidal peperites is a key feature in both Crozon and Buçaco volcanic successions. Peperite is a “genetic term applied to a rock formed essentially in situ by disintegration of magma intruding and mingling with unconsolidated or poorly consolidated, typically wet sediments” (White *et al.* 2000). Fluidal (lobate) clasts are fragmented and mingled in a ductile regime when vapor films along hot magma – cold sediment interfaces, acting as an insulating barrier, prevented direct contact with the pore fluid (Skilling *et al.* 2002). Explosive fragmentation, producing angular fragments, occurs only when the vapor film becomes unstable due to releasing enough kinematic energy to overcome the overburden pressure. Peperites or, more broadly, textures and structures of

sediment/rock domains resulting from interactions between magma and wet sediment, are obvious in all the Rosan/Porto de Santa-Anna sites. The seven most significant facies are:

(1) sediment diapirs or (2) chlorite-bearing pipe vesicles (Fig. 3a, b) at the base of most doleritic sills having (3) lobate morphologies, which are sometimes completely disintegrated *in situ* in the form of (4) amoeboid peperitic clasts within a sedimentary matrix (Caroff *et al.* 2009; Fig. 4); (5) small globular sediment-derived xenoliths dispersed throughout both doleritic sills and sill-derived amoeboid clasts (Fig. 3c, d; Fig. 4); (6) xenolith-bearing fine-textured magmatic planar conduits (or veins) in doleritic sills in Aber, Crozon (Caroff *et al.* 2009; see below); (7) the above-mentioned lobate basaltic clast-bearing rhythmic graded breccia sequence from Lostmarc'h, Crozon (Fig. 4). Caroff *et al.* (2009) have interpreted this latter facies as the results of ductile disintegration of thin sheets of fluid lava by mingling during flowing upon/within unconsolidated sediments, followed by sinking of the largest clasts (a model derived from Brown and Bell 2007). However, it should be noted that the type 7-facies are similar to hyaloclastites formed by quench fragmentation of lava in wet sediments, which can locally display fluidal features as globular peperites (e.g., Caroff 2019). As an example, the Lostmarc'h graded breccia sequence shares some characteristics with the slightly remobilized "peperitic hyaloclastites" from the Pálháza rhyolitic complex, Hungary (Németh *et al.* 2008).

A detailed map of the transition area between the Kermeur and Rosan Formations in the Aber site (Crozon) is shown in Fig. 5. The numerous tectonically verticalized doleritic sills cropping out in this zone display striking water- and/or sediment-related structures. Small sediment diapirs (type 1) occur at the base of sill 2 and 3 (Fig. 5b). Both sills are also characterized by alignments of small chloritic, sediment-derived, globular xenoliths (type 5)

parallel to the sill boundaries (Fig. 5c). We observe in the E–W-oriented sill 4: chlorite-bearing pipe vesicles (type 2) more or less perpendicular to the lower limits (Figs 3a and 5d, e), from which a network of chloritic xenolith-bearing fine-textured magmatic veins (type 6), parallel to the boundaries of the sill at its top and bottom (Fig. 5a, e, g), and plunging to the west at 50–60 degrees in its interior (Fig. 5a, f), extends. Near the upper contact, there are structures resembling, at first sight, basal vesicle pipes (Fig. 5a). In detail, however, there are clear differences between the basal and the upper structures: the upper ones consist of clusters of chloritic xenoliths and vesicles immersed in fine-textured magmatic blobs and topped by upper notches. Note that such blobs also occur a few centimeters underneath the boundary (Fig. 5g).

Most structures of the sill 4 appear to be connected. The magmatic veins carrying chloritic xenoliths (Fig. 5f) seem to originate from basal pipe vesicles (Fig. 3a and Fig. 5d, e) and to end in the upper magmatic blobs/notches (Fig. 5g). The texture of these magmatic segregation products is clearly finer than elsewhere in the sills. The presence of large acicular crystals, sometimes radiating, makes this texture very close to the GDAC one (“Glassy or Doleritic texture with large Acicular Crystals”) defined by Caroff *et al.* (2000) for vesicle cylinders and sheets in vapor-differentiated basalt flows.

## **Mineralogy and geochemistry**

### ***Alteration***

Ejecta, lavas, and intrusions from Crozon/Buçaco have a basaltic composition and contain, as primary groundmass minerals, clinopyroxene, olivine, plagioclase, Fe-Ti oxides, and apatite (Caroff *et al.* 2009), in addition to infrequent (albitized) plagioclase phenocrysts.

Most of them are deeply altered. The primary minerals and glass of the ejecta, which were turning a whitish color, are entirely transformed into quartz, chlorite, oxides, hydroxides and various phyllosilicates, the latter being radially arranged in amygdules, in association with cryptocrystalline quartz. In some basaltic clasts from Aber, we can observe bipyramidal olivine crystals completely transformed into smectite/chlorite and immersed in a chloritized, formerly glassy, matrix (Juteau *et al.* 2007). In the pillow lavas and dolerites, plagioclase is albitized and sericitized, whereas olivine and pyroxene are sometimes entirely converted into assemblages of chlorite, smectite, epidote, titanite and calcite. The altered dolerites have an ochre color, as a result of groundmass hydroxidation (Figs 3a, b; 4; 5c, f).

These alterations and recrystallizations, most of them probably of hydrothermal origin, have preserved the deposit/emplacement delicate primary structures in ejecta and lavas (Juteau *et al.* 2007; Caroff *et al.* 2009). The analytical data for minerals and whole rock samples shown in Supplementary Material (Tables S1, S2, and S3) have been obtained from fresh samples.

### ***Major and trace elements***

To get representative geochemical whole-rock analyses (6 doleritic samples from Crozon and 6 from Buçaco), a 30 g aliquot was homogenized in an agate ball mill. Whole-rock major and trace elements were measured at the PSO/IUEM (Pôle Spectrométrie Océan, Institut Universitaire Européen de la Mer, Brest, France) by inductively coupled plasma-atomic emission spectrometry (ICP-AES) using a Horiba Jobin Yvon Ultima 2<sup>®</sup> spectrometer and following the analytical procedure of Cotten *et al.* (1995). Relative standard deviations are < 2% (< 1% for SiO<sub>2</sub>). The accuracy is better than 7% for Na and P, and better than 3% for the other elements. Weight loss on ignition (LOI) was determined by standard

thermogravimetric technique after heating 500-800 mg of rock powder at 1050 °C for two hours. The error on each measure is  $\leq 2\%$ . Data are shown in Supplementary Material, Table S1.

The geochemical discrimination diagrams  $\log(50V/Ti)$  vs.  $\log(2500Sm/Ti)$  (Fig. 6a) and  $V-Ti/50-5Sc$  (Fig. 6b) from Vermeesch (2006) can be used to determine the paleotectonic context of the Crozon/Buçaco dolerites. All the analyzed Buçaco dolerites have a MORB-type composition, whereas the Crozon dolerites display both MORB and OIB geochemical signatures in diagrams of Fig. 6. The combined occurrence of both MORB- and OIB-type basalts/dolerites is very common in continental intraplate contexts (e.g., Fitton and Upton 1987).

### *Clinopyroxenes in the dolerites*

Groundmass clinopyroxene compositions in 5 doleritic samples from Crozon and 5 from Buçaco were determined using a Cameca SX-100<sup>®</sup> electron microprobe (Microsonde Ouest, Brest, France) with an acceleration voltage of 15kV, a beam current of 20 nA, a counting time of 6 s and a beam diameter of *c.* 1  $\mu\text{m}$ . The corrections were made by the ZAF method. The detection limits are *c.* 0.01% and error is estimated to 1%. Data are shown in Supplementary Material, Table S2.

The pyroxene discrimination diagrams of Leterrier *et al.* (1982) can be used to better define the magmatic affinity of the host dolerites obtained from the whole rock diagrams of Fig. 6. The analyzed clinopyroxene crystals from the Crozon and Buçaco dolerites display anorogenic affinity, mostly falling in the tholeiitic field (Fig. 7). Only the two samples from Kerdreux (Crozon) that plot in the OIB fields of Fig. 6 diagrams include clinopyroxenes with alkaline affinity (Fig. 7a and Supplementary Material, Table S2). Most of the clinopyroxenes

from Crozon and Buçaco have an augitic composition (Fig. 8). The compositions closest to the diopside field correspond to the clinopyroxenes plotting in the alkaline field in the diagram of Fig. 7a. Pigeonite also occurs in one sample from Penacova (Buçaco) (Fig. 8).

### *Phyllosilicates in the metasedimentary xenoliths*

Fresh metasedimentary globular chlorite-rich xenoliths from three doleritic samples from Crozon (Aber) and one from Buçaco (Rio Ceira) were analyzed with a JEOL JSM-5600LV scanning electron microprobe in the IC2MP laboratory of the University of Poitiers (Supplementary Material, Table S3). Quantitative analyses were conducted in high-vacuum mode and with a current tension of 15 kV. The error is estimated to 1%. Furthermore, metasedimentary xenoliths from two doleritic samples (Aber and Rio Ceira) were hand-crushed to powder and the < 2 µm fraction was separated for X-ray diffraction (XRD), to determine structural information at the atomic scale. The samples were studied as oriented powders at the University of Poitiers, using a Philips Panalytical X'pert PRO<sup>®</sup> X-ray diffraction system with Cu-K $\alpha$  radiation ( $\lambda = 0.15418$  nm) operating at 40 kV and 40 mA. XRD analysis was done under air dried, ethylene-glycolated (to highlight some expandable phases), and heated (550 °C) conditions. See Moore and Reynolds (1997) for general information about the XRD procedure and Becker-Kerber *et al.* (2021) for additional methodological details about the IC2MP laboratory.

Phyllosilicates data are shown in the classical  $M^{+}-4Si-R^{2+}$  diagram of Meunier and Velde (1989) of Fig. 9a. The illite(ill)/smectite mixed-layer mineral (I/S MLM) solid solution area is shown, where the smectite component of mixed-layer minerals is a montmorillonite (mnt) whose interlayer charge ranges from 0.33 to 0.66. It appears that the studied phyllosilicates, regardless of their geographic location (Aber or Rio Ceira), are either pure

chlorite or chlorite/smectite (C/S) MLM, the latter having a restricted range of compositions very close to those of the highly chloritic MLM (15-10 % expandable) from the Pliocene felsic pyroclastics / tuffaceous deposits of the Ohyu caldera, Japan (Inoue *et al.* 1984; Meunier *et al.* 1991). Note that other phyllosilicate compositions of comparable metasedimentary xenoliths extracted from other (less fresh) Ordovician igneous bodies (Kerdreux dolerite, Crozon; Plouézec trachy-basalt: Galerne *et al.* 2006) and measured during the same analytical session are very scattered in the  $M^{+}-4Si-R^{2+}$  diagram (Supplementary Material, Fig. S1). In the  $Mg^{2+}$  vs.  $Mg^{2+}/(Mg^{2+}+Fe^{2+}+Mn^{2+})$  diagram of Fig. 9b, the Crozon/Buçaco phyllosilicates are divided into three groups, once again regardless of their geographic location: highly chloritic C/S MLM, low-Mg brunsvigite and high-Mg pycnochlorite/diabantite. In addition, the phyllosilicate XRD patterns of sediment-derived xenoliths from Aber (Fig. 9c) and Rio Ceira (Fig. 9d) are very similar to each other.

## Discussion

### *Formation of the Aber sediment-derived structures*

The occurrence of aligned chloritic xenoliths in the Aber sills (Fig. 5c, f) is one of the most noteworthy features observed in both Rosan/Porto de Santa-Anna volcanic Formations. Caroff *et al.* (2009) suggested that these small globular xenoliths had a sedimentary origin, based on field observations (such as the facies similarity between both sedimentary beds in contact with dolerites and xenoliths, as well as the fact that some chloritic bulges, still attached to their root sedimentary bed, are only partly incorporated in the host intrusive body: Figs 3c and 5a), but they did not investigate the matter any further. The mixed-layer structure of the xenolith phyllosilicates in both Aber (Crozon) and Rio Ceira (Buçaco) is also consistent

with a sedimentary origin. The phyllosilicate features in the two sites are remarkably similar (Fig. 9), suggesting that the sediment composition and the modalities of inclusion into the dolerites are comparable in both sites. Phyllosilicates correspond to sedimentary illite/smectite mixed-layer minerals (I/S MLM) converted into highly chloritic C/S MLM and chlorite probably during the heating associated to the incorporation of the xenoliths, firstly insulated by means of boundary vapor-films, into the intrusions. Schiffman and Fridleifsson (1991) found that the proportion of chlorite in C/S MLM increased continuously with increasing temperature: formation of randomly interstratified chlorite and smectite (C/S) between 200 and 240 °C; formation of both regularly and randomly interstratified C/S between 240 and 264 °C; apparition of discrete chlorite at *c.* 270 °C. Gliozzo (2020) has shown that chlorite is thermally stable in heated clays up to temperature above 850 °C.

The structures observed in the verticalized sills 3 and 4 from Aber (Fig. 5a) combine (i) characteristics of peperites, such as sediment fluidization (Kokelaar 1982; Skilling *et al.* 2002), elutriation (Kwon and Gihm 2017), and sediment diapiring within magmatic bodies (Galerne *et al.* 2006); and (ii) segregations structures observable in vapor-differentiated lava flows, such as pipe vesicles, magmatic vesicle cylinders (Goff 1996), and GDAC texture (Caroff *et al.* 2000). However, the Aber fine-textured magmatic veins are not cylindrical, but more or less planar. If we take as reference the Goff (1996) cylinders, most Aber xenolith-bearing magmatic veins (Fig. 5f) should take root in basal vertical pipes filled with residual magmatic segregation melt, bubbles and fluidized sediment (Fig. 5d, e), then rise as flattened vertical conduits by transferring melt, vapor and sediment from the base of the sills to their upper limit. In this view, the xenolith-bearing fine-textured magmatic blobs associated with notches at the upper edge of some sills would correspond to upper “gas chimney” (Fig. 5g). In such a case, the veins should be perpendicular to the basal sill limit (Goff 1996; Caroff *et al.* 2000). The observed inclination probably means that the segregation magma ascent took place

during laminar flowing of the basaltic magma into the sill channel, as proposed by Elwell *et al.* (1960) and Caroff *et al.* (2011) to explain the formation of inclined segregation pipes in the North-Guernsey Ediacaran gabbro-dioritic pluton. The resulting magmatic shearing could also explain the fact that the Aber segregation conduits have a planar rather than cylindrical shape. The two possible directions of magma flow, by taking the geometry of the inclined veins into account, are shown as 3D-arrows in Fig. 5a.

### ***A tuff cone dynamism***

The detailed study of Crozon volcanoclastics by Caroff *et al.* (2009) enabled them to ascribe the corresponding deposits to the activity of a submarine tuff cone above a < 100 m-deep soft-substrate, with vigorous magmatic injections, persistent interaction of magma with waterlogged sediments, high explosivity, fallout-dominated eruptions and infrequent pyroclastic density currents (e.g., White 1996; Sohn and Park 2005). Tuff cones grow by repeated tephra- and mud-laden jets, which, in watery environments, may initiate tephra fallout, hot turbulent mass flow originated by collapse of eruption column, and sliding/slumping associated with slope collapse (Kano 1998; Kereszturi and Németh 2012; Németh and Kereszturi 2015). The growth of a tuff cone typically includes a pre-emergent and an emergent stage, each producing distinctive facies architecture (Moorhouse *et al.* 2015; Németh and Kereszturi 2015). The basaltic edifice in the Miocene Jinzai Formation (Izumo, Japan), considered by Kano (1998) as a typical shallow-marine tuff cone (above a < 150 m-deep submarine soft-substrate), has the following dimensions: up to 100 m in height above the floor, with a crater 400–500 m wide and a cone rim reaching 1500 m in width, with bedding planes dipping outward at a maximum angle of 20–30°. Flanks were rapidly carved due to syn-eruptive sliding and slumping, followed by a rapid and intense post-eruptive erosion.

The Aber outcrops were interpreted as a cross-section from the root to the lower part of a probably isolated tuff cone (Caroff *et al.* 2009). A hypothetical reconstruction of the pre-emergent volcanic edifice is shown in Fig. 10a. Tephra-laden jets ejected also lime mud (secondary silicified) and water-rich sediment-derived debris. The emergent stage is characterized by increasing slope steepness, which induced subaqueous cold mass flows down the flanks of the cone (Fig. 10b). Water-supported gravity or turbulent mass flows and/or important fallout of blocks and lapilli are thought to produce the crudely stratified volcanoclastic deposits (Facies C of Caroff *et al.* 2009; Fig. 3e). Alternatively, ash-fallout and/or dilute eruption-fed turbidity currents might produce thin-bedded volcanoclastic deposits (Facies D of Caroff *et al.* 2009; Fig. 3f). The hydrovolcanic events were followed by emplacement of pillow lavas and associated rhythmic graded breccia beds, as shown in Fig. 10c.

The poorer outcrop conditions of the Porto de Santa Anna volcanoclastics (Buçaco) do not allow extensive consideration of the volcanological processes in this zone. However, the strong resemblance between Crozon and Buçaco for (i) peperite and tuff facies (Fig. 3), (ii) both volcanic successions (comparable volcanoclastic deposits topped by pillow lavas in both sites: Fig. 4), (iii) whole rock geochemical data (Fig. 6), (iv) clinopyroxene compositions (Figs 7 and 8) and (v) metasedimentary phyllosilicates (Fig. 9) strongly suggest a strict similarity in terms of emplacement modalities, volcanic dynamism, sediment nature and rheology, mineralogy, and magmatic affinity.

### ***Paleogeographic consequences***

The lack of volcanoclastics in the North Crozon unit has been interpreted by Paris (2016) as a consequence of the total abrasion of the Rosan formation in the North unit (Figs

1a, 2) due to sea level fall during the Hirnantian glacial episode. In any case, besides the lack of volcanic breccias, the scarcity of hypabyssal intrusions in the North unit (no sill/dyke in the northern Kermeur formation and rare, narrow peperitic dykes in the northern Postolonnec one, in the same named beach, Fig. 1b), originally located only a few tens of kilometers away from the South one (Caroff *et al.* 2009), is pleading for a very restricted lateral extension of the Upper Katian volcanism complex and its feeder system in Crozon.

The close similarity between the Crozon and Buçaco volcanics, including sediment characteristics and peperitic features, suggest that the two areas would belong to a single monogenetic basaltic field. Modern intraplate volcanic fields contain tens to thousands individual monogenetic cones (Kereszturi and Németh 2012) in areas ranging generally from 50 to 3500 km<sup>2</sup>, exceptionally to 20 000 km<sup>2</sup> (Jaimes-Viera *et al.* 2018). They comprise basaltic edifices with a small cumulative volume, typically  $\leq 1$  km<sup>3</sup> (Németh and Kereszturi 2015). The Crozon/Buçaco volcanoes may have been part of the same volcanic field and grown in identical settings with a common root zone or similar ones (Fig. 10). It follows that both sites were located in close proximity to each other in the Late Ordovician, at a distance ranging from a few kilometers to less than 200-300 km (based on the compilation of modern monogenetic volcanic fields in Jaimes-Viera *et al.* 2018).

The Central Armorican Domain (CAD) and the Central Iberian Zone (CIZ), including the Crozon peninsula and the Buçaco syncline, respectively, are located in the present-day structural map of the European Variscan belt on both sides of the “Ibero-Armorican Arc” (Fig. 11a). This sizeable curved Variscan structure, roughly parallel to the Rheic suture, links together the Armorican and Iberian Massifs (e.g., Authemayou *et al.* 2019). In the Late Ordovician, both domains formed part of the Armorica microplate, as shown in the global Upper Katian paleogeographic reconstruction from Cocks and Torsvik (2021) of Fig. 11b. The close proximity of the Crozon and Buçaco volcanic edifices at that time can be used to

precise the probable position of CAD with respect to CIZ inside the Armorican microplate, as shown in the Fig. 11c magnification.

### ***Late Ordovician limestone, volcanism and climate swings***

The Crozon/Buçaco Ordovician sites are the only zones in North Gondwana where carbonates are associated with volcanism in the same Upper Katian sites (Paris 2016). These limestone beds constitute a sort of anomaly in the Lower Paleozoic siliciclastic succession of the Armorican and Iberian Massifs. They just predated the Hirnantian glaciation, documented in several Gondwanan/peri-Gondwanan regions (Iberian Peninsula, Morocco, Algerian Sahara: Ghienne *et al.* 2007), whose effects resulted locally in the sedimentation of glacio-marine “ball and pillow”-bearing diamictites of the Cosquer (Crozon) and Casal Carvalhal (Buçaco) Formations (Fig. 2). Hirnantian cooling caused sea level to drop significantly, locally leading even to local emersion, like in North Crozon. This carbonate sedimentation is often linked to the “Boda event” as defined by Fortey and Cocks (2005). Following these authors, this sudden appearance of high-latitude carbonate (Fig. 11), accompanied by poleward faunal migrations from equatorial areas, would have marked a global warming event before the latest Hirnantian glaciation and the first severe Phanerozoic mass extinction. Cocks and Torsvik (2021) suggested that the Late Ordovician cooling was driven by decreasing atmospheric CO<sub>2</sub>. Villas *et al.* (2002) proposed that the major triggering factor of the Hirnantian glaciation was the carbonate sedimentation. The accumulation of large amounts of carbonates during the Katian, in peri-Gondwanan regions where such deposits were previously lacking (W- and NE-Armorica, N-Iberia, N-Tripolitania, SW-Sardinia, Carnic Alps, and Thuringia) could have been a major sink of atmospheric CO<sub>2</sub>, which would have produced an important temperature drop in the Lower Hirnantian. Another hypothesis is that

volcanism caused the Late Ordovician climate swings. This has been outlined, for instance, by Bond and Grasby (2020) and Hu et al. (2021), from geochemical data. Major volcanic eruptions in a large igneous province (LIP), maybe Suordakh in eastern Siberia, Russia (Gong *et al.* 2017), would have triggered a long-term deterioration of Late Ordovician environment and climate (cooling in the basal Hirnantian first, then warming and anoxia later in the Hirnantian), causing the final extinction. Of course, the small-volume Katian volcanism in the Crozon/Buçaco area is not directly responsible for such a conjectural global magmatic event.

## Conclusions

1. The Upper Katian anorogenic volcanism from Crozon, in the Central Armorican Domain (CAD), is noteworthy for its magma-sediment mingling and sediment fluidization facies. In particular, some structures combine characteristics of both peperites and magmatic segregations likely to derive from vapor-differentiation, such as magmatic vesicle veins carrying small sediment-derived globular xenoliths.
2. The Crozon deposits are inferred to have resulted from the activity of a submarine tuff cone above a < 100 m-deep soft-substrate. This hydrovolcanic activity was followed by emplacement of pillow lavas and rhythmic graded breccia beds.
3. The coeval Buçaco volcanics, in the Central Iberian Zone (CIZ), display peperite and tuff facies akin to the Crozon ones. Volcanic stratigraphies are identical, together with their mineralogical and geochemical compositions. The hypabyssal bodies from the two localities contain comparable metasedimentary xenoliths, whose high temperature phyllosilicates have a very restricted range of compositions. All this suggests a strict likeness between both sites in terms of

emplacement modalities, volcanic dynamism, sediment nature, and magmatic affinity.

4. The very close geographical proximity of the Crozon and Buçaco Late Ordovician volcanoes, likely within the boundaries of a single monogenetic basaltic field, can be used to precise the position of CAD with respect to CIZ inside the Armorican microplate at that time.
5. The CAD and CIZ are the only areas in North Gondwana where carbonates are associated with volcanism in the same Katian outcrops. This sudden apparition of high-latitude carbonate would have marked a global warming just before the Gondwanan Hirnantian glaciation and the first Phanerozoic mass extinction.

### **Acknowledgements**

The site of Crozon will be part of the future Armorique Geopark supported by both the Armorique Regional Nature Park (PNRA: J.-J. Barreau, Director; J. Bourdoulous, Director of natural heritage; N. Courant, Geopark Coordinator) and the Regional Nature Reserve of the Crozon Peninsula (S. Coat, Curator). This research project was funded by the Géo-Océan Laboratory, IUEM, Brest (France). Field studies were achieved in Buçaco (Portugal) in November 2008 and February 2010, with M. Vidal, M. Thomas, M.-P. Dabard (deceased), A. Loi, and R. Gourvennec, and in Crozon (France) from 2009 to 2011 with M. Thomas. The authors are grateful to M. Thomas for her field contribution and her participation to the electron microprobe sessions and to F. Haurine for his participation to the scanning electron microprobe and XRF sessions at the IC2MP laboratory (University of Poitiers), as part of their Master's projects in the University of Brest. The author thanks M. Vidal (Géo-Océan Laboratory, for fruitful discussion on Ordovician stratigraphy), P. Dudoignon and A. Meunier (scanning electron microprobe and XRF, IC2MP laboratory, University of Poitiers), J.

Langlade (microprobe analyses, Géo-Océan Laboratory), C. Liorzou (ICP-AES, Géo-Océan Laboratory), P. Tieffenbach (thin sections, Géo-Océan Laboratory), and J.-P. Oldra (sample preparation, Géo-Océan Laboratory). Detailed and constructive comments by Drs K. Németh and Y.K. Sohn helped me a lot to improve the first version of the text. The author thanks also Dr. L. Fedele for his editorial handling

## References

- Authemayou, C., Le Gall, B., Caroff, M. and Bussien Grosjean, D. 2019. Wrench-related dome formation and subsequent orogenic syntax bending in a hot orogen (Variscan Ibero-Armorican Arc, the Ouessant Island, France). *Tectonics*, **38**, <https://doi.org/10.1029/2018TC005189>.
- Becker-Kerber, B., El Albani, A., Konhauser, K. *et al.* 2021. The role of volcanic-derived clays in the preservation of Ediacaran biota from the Itajaí Basin (ca. 563 Ma, Brazil). *Scientific Reports*, **11**, 5013, <https://doi.org/10.1038/s41598-021-84433-0>.
- Bond, D.P.G. and Grasby, S.E. 2020. Late Ordovician mass extinction caused by volcanism, warming, and anoxia, not cooling and glaciation. *Geology*, **48**, 777–781, <https://doi.org/10.1130/G47377.1>.
- Brown, D.J. and Bell, B.R. 2007. How do you grade peperites? *Journal of Volcanology and Geothermal Research*, **159**, 409–420, <https://doi.org/10.1016/j.jvolgeores.2006.08.008>.
- Caroff, M. 2019. Emplacement of lobate sheet flows with hyaloclastites onto soft sediment: The Erquy Neoproterozoic lava pile, Armorican Massif (France). *Precambrian Research*, **334**, 105454, <https://doi.org/10.1016/j.precamres.2019.105454>.
- Caroff, M., Barrat, J.-A. and Le Gall, B. 2021. Kersantites and associated intrusives from the type locality (Kersanton), Variscan Belt of Western Armorica (France). *Gondwana Research*, **98**, 46–62, <https://doi.org/10.1016/j.gr.2021.06.004>.

- Caroff, M., Coint, N., Hallot, E., Hamelin, C., Peucat, J.-J. and Charreteur, G. 2011. The mafic–silicic layered intrusions of Saint-Jean-du-Doigt (France) and North-Guernsey (Channel Islands), Armorican Massif: Gabbro–diorite layering and mafic cumulate–pegmatoid association. *Lithos*, **125**, 675–692, <https://doi.org/10.1016/j.lithos.2011.03.019>.
- Caroff, M., Maury, R.C., Cotten, J. and Clément, J.P. 2000. Segregation structures in vapor-differentiated basaltic flows. *Bulletin of Volcanology*, **62**, 171–187, <https://doi.org/10.1007/s004450000077>.
- Caroff, M., Vidal, M., Bénard, A. and Darboux, J.-R. 2009. A late-Ordovician phreatomagmatic complex in marine soft-substrate environment: The Crozon volcanic system, Armorican Massif (France). *Journal of Volcanology and Geothermal Research*, **184**, 351–366, <http://doi.org/10.1016/j.jvolgeores.2009.05.002>.
- Cocks, L.R.M. and Torsvik, T.H. 2021. Ordovician palaeogeography and climate change. *Gondwana Research*, **100**, 53–72, <http://doi.org/10.1016/j.gr.2020.09.008>.
- Colmenar, J., Pereira, S., Pires, M., Silva (da), C.M., Sá, A.A. and Young, T.P. 2017a. A Kralodvorian (upper Katian, Upper Ordovician) benthic association from the Ferradosa Formation (Central Portugal) and its significance for the redefinition and subdivision of the Kralodvorian Stage. *Bulletin of Geosciences*, **92**(4), 443–464, <https://doi.org/10.3140/bull.geosci.1643>.
- Colmenar, J., Pereira, S., Sá, A.A., Pires, M., Silva (da), C.M. and Young, T.P. 2017b. The highest-latitude *Foliomena* Fauna (Upper Ordovician, Portugal) and its palaeogeographical and palaeoecological significance. *Palaeogeography, Palaeoclimatology, Palaeoecology*, **485**, 774–783, <http://doi.org/10.1016/j.palaeo.2017.07.035>.

- Colmenar, J., Pereira, S., Young, T.P., Silva (da), C.M. and Sá, A.A. 2019. First report of Hirnantian (Upper Ordovician) high-latitude peri-gondwanan macrofossil assemblages from Portugal. *Journal of Paleontology*, **93**(3), 460–475, <https://doi.org/10.1017/jpa.2018.88>.
- Cotten, J., Le Dez, A., Bau, M., Caroff, M., Maury, R., Dulski, P., Fourcade, S., Bohn, M. and Brousse, R. 1995. Origin of rare-earth element and yttrium enrichments in subaerial exposed basalts: evidence from French Polynesia. *Chemical Geology*, **119**, 115–138, [https://dx.doi.org/10.1016/0009-2541\(94\)00102-E](https://dx.doi.org/10.1016/0009-2541(94)00102-E).
- Crowley, Q.G., Floyd, P.A., Winchester, J.A., Franke, W. and Holland, J.G. 2000. Early Palaeozoic rift-related magmatism in Variscan Europe: fragmentation of the Armorican Terrane Assemblage. *Terra Nova*, **12**, 171–180, <https://doi.org/10.1046/j.1365-3121.2000.00290.x>.
- Elwell, R.W.D., Skelhorn, R.R. and Drysdall, A.R. 1960. Inclined granitic pipes in the diorites of Guernsey. *Geological Magazine*, **97**, 89–105.
- Fernández-Suárez, J, Gutiérrez Alonso, G., Cox, R. and Jenner, G.A. 2002. Assembly of the Armorica Microplate: A strike-slip terrane delivery? Evidence from U-Pb ages of detrital zircons. *Journal of Geology*, **110**, 619–626, <https://doi.org/10.1086/341760>.
- Fitton, J.G. and Upton, B.G.J. (eds), 1987. Alkaline Igneous Rocks. *Geological Society Special Publications*, **30**, ix–xiv.
- Fortey, R.A. and Cocks, L.R.M. 2005. Late Ordovician global warming – The Boda event. *Geology*, **33**, 405–408, <https://doi.org/10.1130/G21180.1>.
- Fortey, R.A. and Cocks, L.R.M., 2003. Palaeontological evidence bearing on Ordovician-Silurian continental reconstructions. *Earth-Science Reviews*, **61**, 245–307, [https://doi.org/10.1016/S0012-8252\(02\)00115-0](https://doi.org/10.1016/S0012-8252(02)00115-0).

- Franke, W., Cocks, L.R.M. and Torsvik, T.H. 2017. The Palaeozoic Variscan oceans revisited. *Gondwana Research*, **48**, 257–284, <https://doi.org/10.1016/j.gr.2017.03.005>.
- Galerie, C., Caroff, M., Rolet, J. and Le Gall, B. 2006. Magma–sediment mingling in an Ordovician rift basin: The Plouézec–Plourivo half-graben, Armorican Massif, France. *Journal of Volcanology and Geothermal Research*, **155**, 164–178, <https://doi.org/10.1016/j.jvolgeores.2006.03.030>.
- Ghienne J.F., Boumendjel K., Paris F., Videt B., Racheboeuf P. and Aït Salem H. 2007. The Cambrian-Ordovician succession in the Ougarta Range (western Algeria, North Africa) and interference of the Late Ordovician glaciation on the development of the Lower Palaeozoic transgression on northern Gondwana. *Bulletin of Geosciences*, **82**, 183–792, <https://doi.org/10.3140/bull.geosci.2007.03.183>.
- Gliozzo, E. 2020. Ceramic technology. How to reconstruct the firing process. *Archaeological and Anthropological Sciences*, **12**, 260, <https://doi.org/10.1007/s12520-020-01133-y>.
- Goff, F. 1996. Vesicle cylinders in vapor-differentiated basalt flows. *Journal of Volcanology and Geothermal Research*, **71**, 167–185, [https://doi.org/10.1016/0377-0273\(95\)00073-9](https://doi.org/10.1016/0377-0273(95)00073-9).
- Gong, Q., Wang, X., Zhao, L., Grasby, S.E., Chen, Z.-Q., Zhang, L., Li, Y., Cao, L. and Li, Z. 2017. Mercury spikes suggest volcanic driver of the Ordovician-Silurian mass extinction. *Scientific Reports*, **7**, 5304, <https://doi.org/10.1038/s41598-017-05524-5>.
- Henry, J.L., Mélou, M., Nion, J., Paris, F., Robardet, M., Skevington, D. and Thadeu, D. 1976. L'apport de graptolites de la zone à *G. teretiusculus* dans la datation de faunes benthiques lusitoarmoricaïnes. *Annales de la Société géologique du Nord*, **96**, 275–281.
- Henry, J.L., Nion, J., Paris, F. and Thadeu, D. 1974. Chitinozoaires, ostracodes et trilobites de l'Ordovicien du Portugal (Serra de Buçaco) et du Massif armoricain : essai de comparaison et signification paléogéographique. *Comunicações dos Serviços Geológicos de Portugal (1973-1974)*, **57**, 303–345.

- Hey, M.H. 1954. A new review of the chlorites. *Mineralogical Magazine*, **30**, 277–292, <https://doi.org/10.1180/minmag.1954.030.224.01>.
- Hu, D., Li, M., Chen, J., Luo, Q., Grasby, S.E., Zhang, T., Yuan, S., Xu, Y., Finney, S.C., Sun, L. and Shen, Y. 2021. Major volcanic eruptions linked to the Late Ordovician mass extinction: Evidence from mercury enrichment and Hg isotopes. *Global and Planetary Change*, **196**, 103374, <https://doi.org/10.1016/j.gloplacha.2020.103374>.
- Inoue, A., Utada, M., Nagata, H. and Watanabe, T. 1984. Conversion of trioctahedral smectite to interstratified chlorite/smectite in Pliocene acidic pyroclastic sediments of the Ohyu District, Akita Prefecture, Japan. *Clay Science*, **6**, 130–116, <https://doi.org/10.11362/jcssjclayscience1960.6.103>.
- Jaimes-Viera, M.C., Martin Del Pozzo, A.L., Layer, P.W., Benowitz, J.A. and Nieto-Torres, A. 2018. Timing the evolution of a monogenetic volcanic field: Sierra Chichinautzin, Central Mexico. *Journal of Volcanology and Geothermal Research*, **356**, 225–242, <https://doi.org/10.1016/j.jvolgeores.2018.03.013>.
- Juteau T., Nonnotte P., Jegou I., Lamour, M., Naour, T. and Cotten, J. 2007. Le volcanisme sous-marin d'âge ordovicien supérieur de la presqu'île de Crozon (Finistère). Étude des processus de bréchification. *Bulletin de la Société Géologique et Minéralogique de Bretagne*, **D(4)**, 1–67.
- Kano, K. 1998. A shallow-marine alkali-basalt tuff cone in the Middle Miocene Jinzai Formation, Izumo, SW Japan. *Journal of Volcanology and Geothermal Research*, **87**, 173–191, [https://doi.org/10.1016/S0377-0273\(98\)00098-5](https://doi.org/10.1016/S0377-0273(98)00098-5).
- Kokelaar, B.P. 1982. Fluidization of wet sediments during emplacement and cooling of various igneous rocks. *Journal of Geological Society, London*, **139**, 21–33, <http://dx.doi.org/10.1144/gsjgs.139.1.0021>.

- Kereszturi, G. and Németh, K. 2012. Monogenetic Basaltic Volcanoes: Genetic Classification, Growth, Geomorphology and Degradation. In: Updates in Volcanology - New Advances in Understanding Volcanic Systems, IntechOpen.  
<https://doi.org/10.5772/51387>.
- Kwon, C.W. and Gihm, Y.S. 2017. Fluidization of host sediments and its impacts on peperites-forming processes, the Cretaceous Buan Volcanics, Korea. *Journal of Volcanology and Geothermal Research*, **341**, 84–93,  
<http://dx.doi.org/10.1016/j.jvolgeores.2017.05.019>.
- Lefebvre, V., Servais, T., François, L. and Averbuch, O. 2010. Did a Katian large igneous province trigger the Late Ordovician glaciation? A hypothesis tested with a carbon cycle model *Palaeogeography, Palaeoclimatology, Palaeoecology*, **296**, 310–319,  
<https://doi.org/10.1016/j.palaeo.2010.04.010>.
- Le Gall, B., Authemayou, C., Graindorge, D., Duperret, A., Tassadit, K., Ehrhold, A. and Schmitt, T. 2021. Status of Basement Terranes in Orogens: Insights From the Cadomian Domain of the North Armorican Variscides, Western France. *Tectonics*, **40**, e2020TC006578, <https://doi.org/10.1029/2020TC006578>
- Leterrier, J., Maury, R.C., Thonon, P., Girard, D. and Marchal, M. 1982. Clinopyroxene composition as a method of identification of the magmatic affinities of paleo-volcanic series. *Earth and Planetary Science Letters*, **59**(1), 139–154,  
[https://doi.org/10.1016/0012-821X\(82\)90122-4](https://doi.org/10.1016/0012-821X(82)90122-4).
- Matte, P. 2001. The Variscan collage and orogeny (480–290 Ma) and the tectonic definition of the Armorica microplate: a review. *Terra Nova*, **13**(2), 122–128,  
<https://doi.org/10.1046/j.1365-3121.2001.00327.x>.

- Meunier, A., Inoue, A. and Beaufort, D. 1991. Chemiographic Analysis of Trioctahedral Smectite-to-Chlorite Conversion Series from the Ohyu Caldera, Japan. *Clays and Clay Minerals*, **39**, 409–415, <https://doi.org/10.1346/CCMN.1991.0390410>.
- Meunier, A. and Velde, B. 1989. Solid solutions in I/S mixed-layer minerals and illite. *American Mineralogist*, **74**, 1106–1112.
- Moore, D.M. and Reynolds, R.C. Jr. 1997. X-Ray Diffraction and the Identification and Analysis of Clay Minerals (2<sup>nd</sup> ed.). New York, Oxford University Press, 378 p.
- Moorhouse, B.L., White, J.D.L. and Scott, J.M. 2015. Cape Wanbrow: A stack of Surtseyan-style volcanoes built over millions of years in the Waiareka–Deborah volcanic field, New Zealand. *Journal of Volcanology and Geothermal Research*, **298**, 27–46, <http://dx.doi.org/10.1016/j.jvolgeores.2015.03.019>.
- Morimoto, N., Fabries, J., Ferguson, A.K., Ginzburg, I.V., Ross, M., Seifert, F.A., Zussman, J., Aoki, K. and Gottardi, G. 1988. Nomenclature of pyroxenes. *Mineralogical Magazine*, **52**(367), 535–550, <https://doi.org/10.1180/minmag.1988.052.367.15>.
- Németh, K. and Kereszturi, G. 2015. Monogenetic volcanism: personal views and discussion. *International Journal of Earth Sciences*, **104**, 2131–2146, <https://doi.org/10.1007/s00531-015-1243-6>.
- Németh, K., Pécskay, Z., Martin, U., Gméling, K., Molnár, F. and Cronin, S.J. 2008. Hyaloclastites, peperites and soft-sediment deformation textures of a shallow subaqueous Miocene rhyolitic dome-cryptodome complex, Pálháza, Hungary. In: Thomson, K., Petford, N. (Eds), Structure and emplacement of high-level magmatic systems. *Geological Society, London, Special Publications*, **302**, 61–83, <https://doi.org/10.1144/SP302.5>.
- Oliveira, J.T., Pereira, E., Piçarra, J.M., Young, T. and Romano, M. 1992. O Paleozóico Inferior de Portugal: Síntese da estratigrafia e da evolução paleogeográfica. In: Gutiérrez

- Marco, J.G., Saavedra, J., Rábano, I. (Eds), Paleozoico Inferior de Ibero-Armorica. Universidad de Extremadura, 359–375.
- Paris, F. 2016. L'Ordovicien du domaine médio-nord-armoricain : contexte paléogéographique. In : Trilobites de l'Ordovicien breton et faune associée. *Fossiles*, **HS 7**, 5–20.
- Paris, F., Pelhate, A. and Weyant, M. 1981. Conodontes ashgilliens dans la Formation de Rosan, coupe de Lostmarc'h (Finistère, Massif armoricain). Conséquences paléogéographiques. *Bulletin de la Société Géologique et Minéralogique de Bretagne*, (C) **XIII** (2), 15–35.
- Paris, F. and Robardet, M. 1977. Paléogéographie et relations ibéro-armoricaines au Paléozoïque anté-carbonifère. *Bulletin de la Société géologique de France*, **19** (5), 1121–1126, <https://doi.org/10.2113/gssgfbull.S7-XIX.5.1121>.
- Plusquellec Y., with the collaboration of Chauvel J.-J., Darboux J.-R., Gourvennec R., Hallegouet B., Le Herisse A., Morzadec P., Paris F. and Vidal., M. 2010. Curiosités géologiques de la presqu'île de Crozon. BRGM, Orléans / Apogée, Rennes / SGMB, Rennes.
- Robardet, M. 2003. The Armorica 'microplate': fact or fiction? Critical review of the concept and contradictory palaeobiogeographical data. *Palaeogeography, Palaeoclimatology, Palaeoecology*, **195** (1–2), 125–148, [https://doi.org/10.1016/S0031-0182\(03\)00305-5](https://doi.org/10.1016/S0031-0182(03)00305-5).
- Robardet, M. and Gutierrez Marco, J.C. 1990. Sedimentary and Faunal Domains in the Iberian Peninsula During Lower Paleozoic Times. In: Dallmeyer R.D., Garcia E.M. (Eds), Pre-Mesozoic Geology of Iberia, IGCP-Project 233 (Terranes in the Circum-Atlantic Paleozoic Orogens), Springer, Berlin, Heidelberg, [https://doi.org/10.1007/978-3-642-83980-1\\_27](https://doi.org/10.1007/978-3-642-83980-1_27).

- Robardet, M., Paris, F. and Racheboeuf, P.R. 1990. Palaeogeographic evolution of southwestern Europe during Early Palaeozoic times. In: McKerrow, W.S., Scotese, C.R. (Eds), Palaeozoic Palaeogeography and Biogeography. *Geological Society, London, Memoirs*, **12**, 411–419.
- Sá, A.A., Piçarra, J., Vaz, N., Sequira, A. and Gutiérrez-Marco, J.C. 2011. Ordovician of Portugal. In: 11th International Symposium on the Ordovician System, Pre-Conference Field Trip Guide. Universidade de Trás-os-Montes e Alto Douro–CSIC–Museo Geominero, Alcalá de Henares.
- Schiffman, P. and Fridleifsson, G.O. 1991. The smectite–chlorite transition in drillhole NJ-15, Nesjavellir geothermal field, Iceland: XRD, BSE and electron microprobe investigations. *Journal of Metamorphic Geology*, **9**, 679–696, <https://doi.org/10.1111/j.1525-1314.1991.tb00558.x>.
- Skilling, I.P., White, J.D.L. and McPhie, J. 2002. Peperite: a review of magma–sediment mingling. *Journal of Volcanology and Geothermal Research*, **114**(1-2), 1–17, [https://doi.org/10.1016/S0377-0273\(01\)00278-5](https://doi.org/10.1016/S0377-0273(01)00278-5).
- Sohn, Y.K. and Park, K.H. 2005. Composite tuff ring/cone complexes in Jeju Island, Korea: possible consequences of substrate collapse and vent migration. *Journal of Volcanology and Geothermal Research*, **141**, 157–175, <https://doi.org/10.1016/j.jvolgeores.2004.10.003>.
- Vermeesch, P. 2006. Tectonic discrimination diagrams revisited. *Geochemistry, Geophysics, Geosystems*, **7**, Q06017, <https://doi.org/10.1029/2005GC001092>.
- Vidal, M., Dabard, M.-P., Gourvenec, R., Le Hérisse, A., Loi, A., Paris, F., Plusquellec, Y. and Recheboeuf, P.R. 2011. Le Paléozoïque de la presqu’île de Crozon, Massif armoricain (France). *Géologie de la France*, **1**, 3–45.

- Villas, E., Vennin, E., Álvaro, J.J., Hammann, W., Herrera, Z.A. and Piovano, E.L. 2002. The late Ordovician carbonate sedimentation as a major triggering factor of the Hirnantian glaciation. *Bulletin de la Société Géologique de France*, **173**(6), 569–578, <https://doi.org/10.2113/173.6.569>.
- White, J.D.L. 1996. Impure coolants and interaction dynamics of phreatomagmatic eruptions. *Journal of Volcanology and Geothermal Research*, **165**, 1–17, [https://doi.org/10.1016/S0377-0273\(96\)00061-3](https://doi.org/10.1016/S0377-0273(96)00061-3).
- White, J.D.L., McPhie, J. and Skilling, I.P. 2000. Peperite: a useful genetic term. *Bulletin of Volcanology*, **62**, 65–66, <https://doi.org/10.1007/s004450050293>.
- Young, T.P. 1988. The lithostratigraphy of the upper Ordovician of central Portugal. *Journal of the Geological Society*, **145**, 377–392, <https://doi.org/10.1144/gsjgs.145.3.0377>.

#### FIGURE CAPTIONS

Figure 1. (a) Sketch geological map of the Crozon Peninsula, Armorican Massif, France, from Plusquellec (2010). (b) Sketch geological map of the southern part of the Crozon Peninsula, from Plusquellec (2010) and Vidal *et al.* (2011). (c) Portugal map showing the Ordovician outcrops, from Colmenar *et al.* (2019). (d) Sketch geological map of the Buçaco Syncline, from Colmenar *et al.* (2019).

Figure 2. Chronolithostratigraphic correlation columns between Crozon (France) and North Buçaco (Portugal). Crozon column from Paris *et al.* (1981), Plusquellec (2010), Vidal *et al.* (2011), and Caroff *et al.* (2009). North Buçaco column compiled and synthesized from Young (1988), Robardet *et al.* (1990), Oliveira *et al.* (1992), Sá *et al.* (2011), and Colmenar *et al.* (2017a, b; 2019).

Figure 3. Photographs of magmatic samples from Aber, Crozon (a, c, e, f) and Galhano, Buçaco (b, d, g). (a) (b) Aber/Galhano pipe vesicles at the base of doleritic sills. (c) (d) Aber/Galhano globular sediment-derived chloritic xenoliths in doleritic sills. (e) (f) (g) Aber/Galhano volcanoclastic deposits (facies C and D of Caroff *et al.* 2009). See text for explanations.

Figure 4. Lithostratigraphic columns of the Katian volcanic succession in Crozon (France) and North Buçaco (Portugal), showing the correlations between the Aber/Lostmarc'h sites in the Crozon Peninsula (modified from Caroff *et al.* 2009) and the Cabeço Pedrogão/Galhano sites in the Buçaco Syncline (Galhano: modified from Young 1988; Cabeço Pedrogão: new data).

Figure 5. (a) Detailed geological map of the transition area between the Kermeur and Rosan Formations in the Aber site. The doleritic sills crop out in vertical position. 3D-arrows indicate the two possible directions of magma flow. (b) (d) (e) (g) Gray: host dolerites; pale gray: magmatic segregation products (pipes, veins, and blobs); black: sediment-derived chloritic material (sediment diapirs, pipes, and xenoliths). (b) Photograph of sediment diapirs at the base of the doleritic sill 3. (c) Photograph of globular/lobate sediment-derived xenoliths at the upper part of the doleritic sill 3. (d) (e) Sketches of pipes vesicles at the base of the doleritic sill 4 and fine-textured horizontal veins, filled with residual magmatic segregation melt (pale gray), bubbles (white) and fluidized sediment (black). (f) Photographs of inclined fine-textured magmatic veins (yellow ochre) carrying sediment-derived chloritic xenoliths (black) through the doleritic sill 4. (g) Sketch of a fine-textured magmatic horizontal vein

(lower part, in pale gray), bubble- and xenolith-bearing magmatic blobs (upper part, in pale gray), and top notches (“gas chimneys”?) at the upper edge of the doleritic sill 4.

Figure 6. Geochemical discrimination diagrams (in ppm) from Vermeesch (2006): (a)  $\log(50V/Ti)$  vs.  $\log(2500Sm/Ti)$ ; (b)  $V-Ti/50-5Sc$ . OIB: ocean island basalts; MORB: mid-ocean ridge basalts; IAB: island arc basalts.

Figure 7. Discrimination diagram for clinopyroxenes from Crozon and Buçaco sills from Letierrier et al. (1982). (a) Ti vs. Ca + Na, discriminating alkaline vs. tholeiitic/calc-alkaline basalts/dolerites and (b) Ti + Cr vs. Ca, discriminating anorogenic tholeiites vs. orogenic basalts/dolerites. The clinopyroxenes plotting in the alkaline field in (a), not shown in (b), belong to the two dolerite samples from Kerdreux (Crozon) plotting in the OIB fields in both diagrams of Fig. 6.

Figure 8. Pyroxene classification diagram illustrating the compositional variation in the groundmass pyroxenes of doleritic sills from Crozon and Buçaco (sampling sites in Supplementary Material, Table S2). Nomenclature after Morimoto (1988).

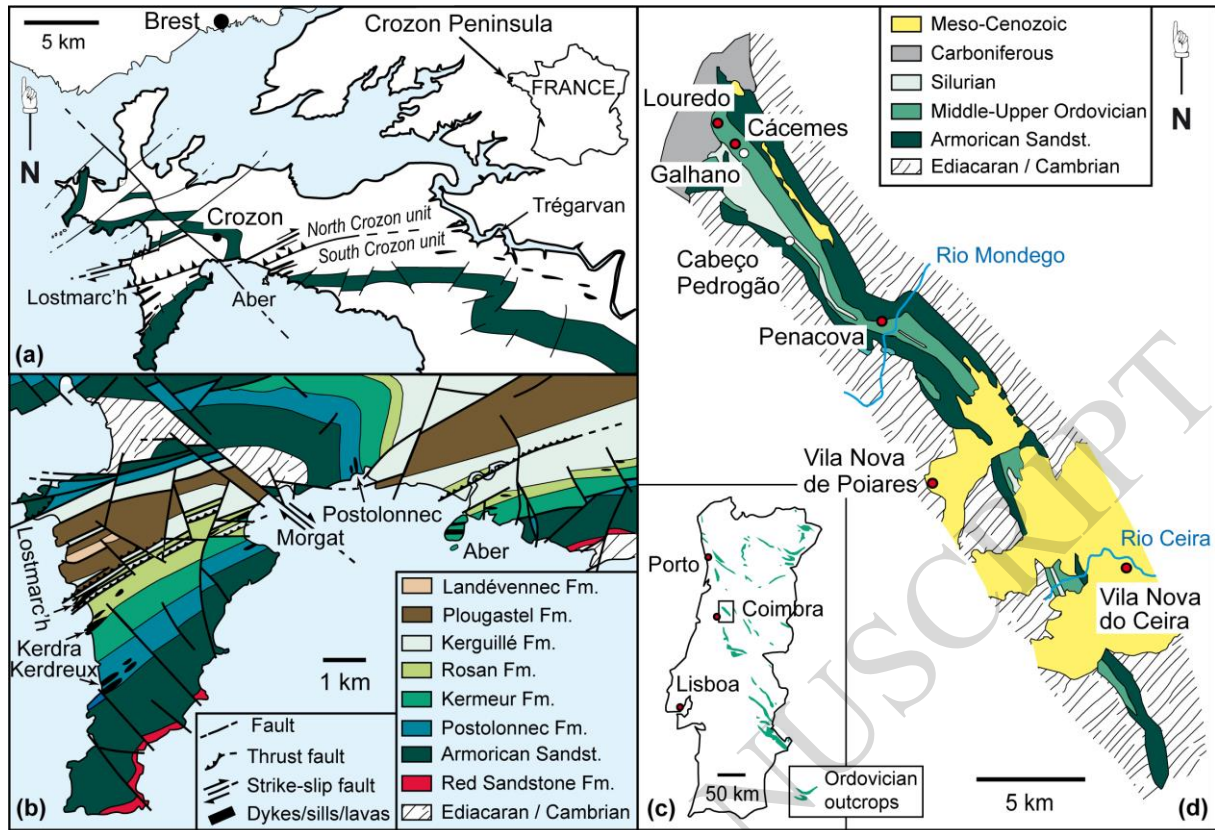
Figure 9. Phyllosilicate composition in sediment-derived xenoliths of doleritic sills from Aber (Crozon) and Rio Ceira (Buçaco). (a)  $M^+ - 4Si - R^{2+}$  diagram of Meunier and Velde 1989, where the  $M^+$  pole ( $= Na^+ + K^+ + 2Ca^{2+}$ ) indicates the layer charge of ideal mica, the 4Si pole ( $= Si^{4+}/4$ ) represents the maximum Si content of the tetrahedral sheet, and the  $R^{2+}$  pole ( $= Mg^{2+} + Fe^{2+} + Mn^{2+}$ ) corresponds to the amount of bivalent cations in the octahedral position. (I/S, C/S) MLM: (illite/smectite, chlorite/smectite) mixed-layer minerals; ill: illite; mnt: montmorillonite; be: beidellite. C/S MLM compositions of slightly metamorphosed

pyroclastics from the Ohyu caldera formation (Japan) are indicated for comparison, divided into three groups, with their respective expandability (Inoue *et al.* 1984; Meunier *et al.* 1991). (b)  $\text{Mg}^{2+}$  vs.  $\text{Mg}^{2+}/(\text{Mg}^{2+}+\text{Fe}^{2+}+\text{Mn}^{2+})$  diagram (nomenclature of Hey 1954). (c) (d) XRD patterns of oriented powder of sediment-derived xenoliths from Aber (c) and Rio Ceira (d), for three different sample preparation methods. Sm: smectite; Ch: chlorite. Gray labels above peaks denote d-spacing in nanometers.

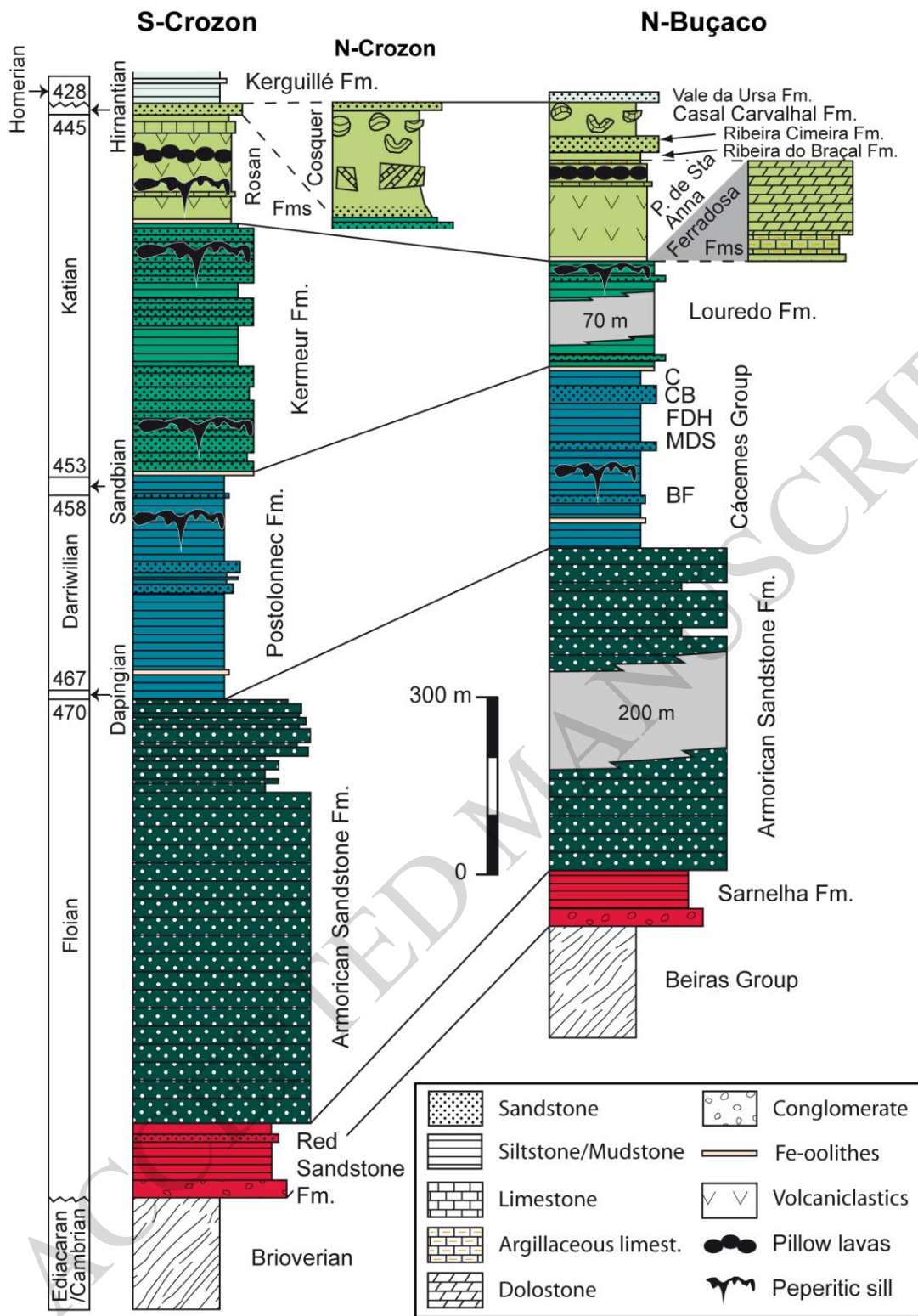
Figure 10. Schematic representation of the evolution of the Crozon/Buçaco Surtseyan-type complex. Reconstructions modified from Caroff *et al.* (2009) and based on Kano (1998), Kereszturi and Németh (2012), Moorhouse *et al.* (2015), and Németh and Kereszturi (2015). Depths have been estimated in Crozon from sedimentological and palaeontological/taphonomic observations in the limestone beds (Caroff *et al.* 2009). Black: basaltic/doleritic material (intrusions, pillow lavas, clasts); gray: sediment-derived clasts; white: sediment-derived pipes and xenoliths. (a) Pre-emergent stage, with fully subaqueous tephra-laden jets, high-density eruption-fed water-supported current, and traction-dominated sedimentation. Dykes and sills intruded the surrounding soft substrate and the volcanoclastic deposits after they had incorporated sedimentary xenoliths in the course of their progression. The morphology of the peperitic intrusions at different paleo-depths suggests that the substrate was less hydrated and more cemented deep down, but not completely lithified. (b) Stabilized volcanic edifice after partial emersion, subsequent to several events such as high-energy jets, eruption-fed submarine turbidity currents and sliding/slumping episodes. (c) Volcano section just after the end of the volcanic activity. Pillow lavas and associated graded brecciated beds (observed only in Crozon) postdate the Surtseyan events.

Figure 11. (a) Structural map and main tectonostratigraphic units of the European Variscan belt (modified from Caroff *et al.* 2021; see references herein). CAD: Central Armorican Domain (Armorican Massif); CIZ: Central Iberian Zone (Iberian Massif). (b) Global paleogeography of Later Ordovician (Upper Katian) lands and oceans at about 450 Ma, modified from Cocks and Torsvik (2021). Lambert azimuthal equal area projection centered on the South Pole. High latitude carbonates (Boda event) from Fortey and Cocks (2005). (c) Upper Katian position of both CAD and CIZ. B. Buçaco; C. Crozon.

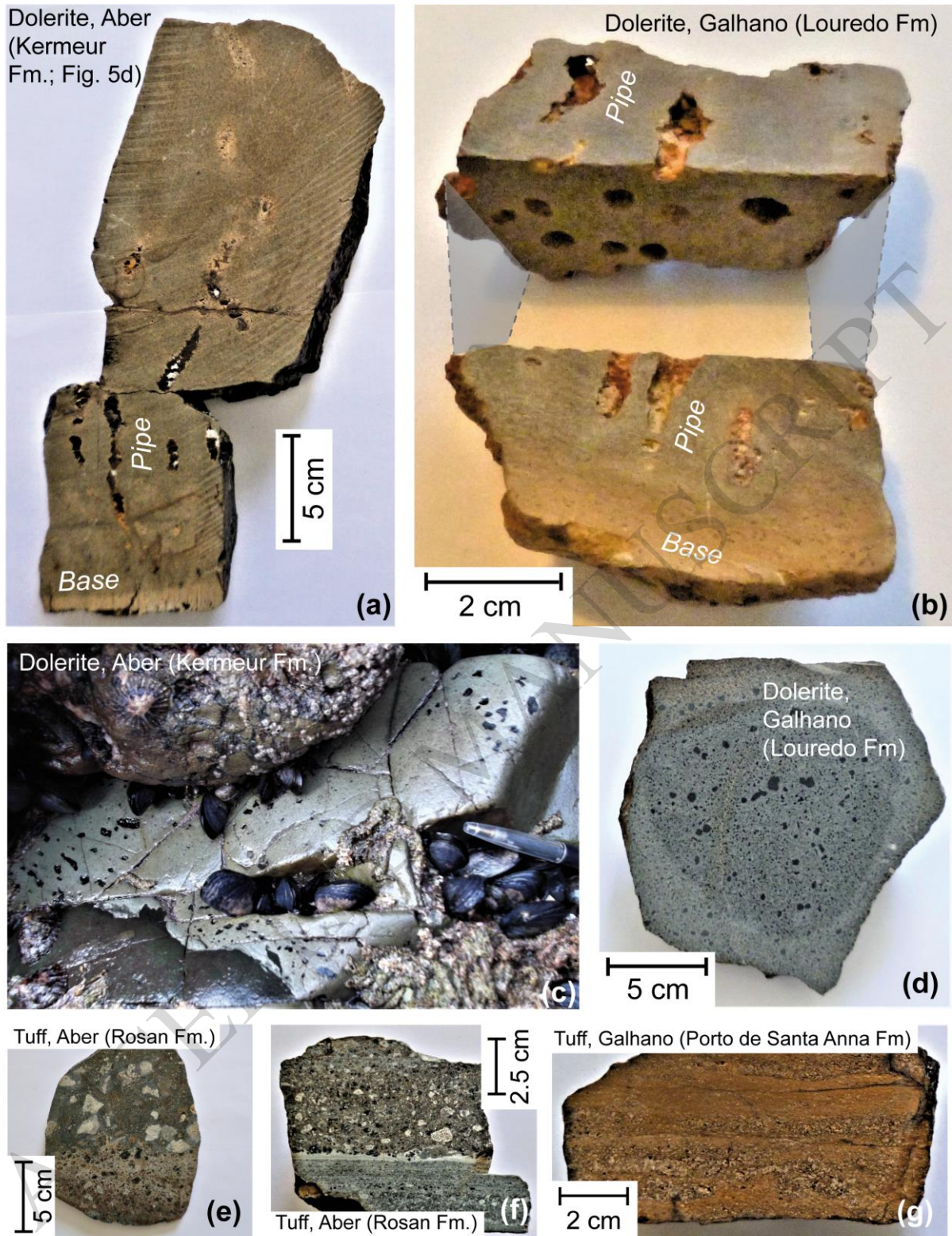
ACCEPTED MANUSCRIPT



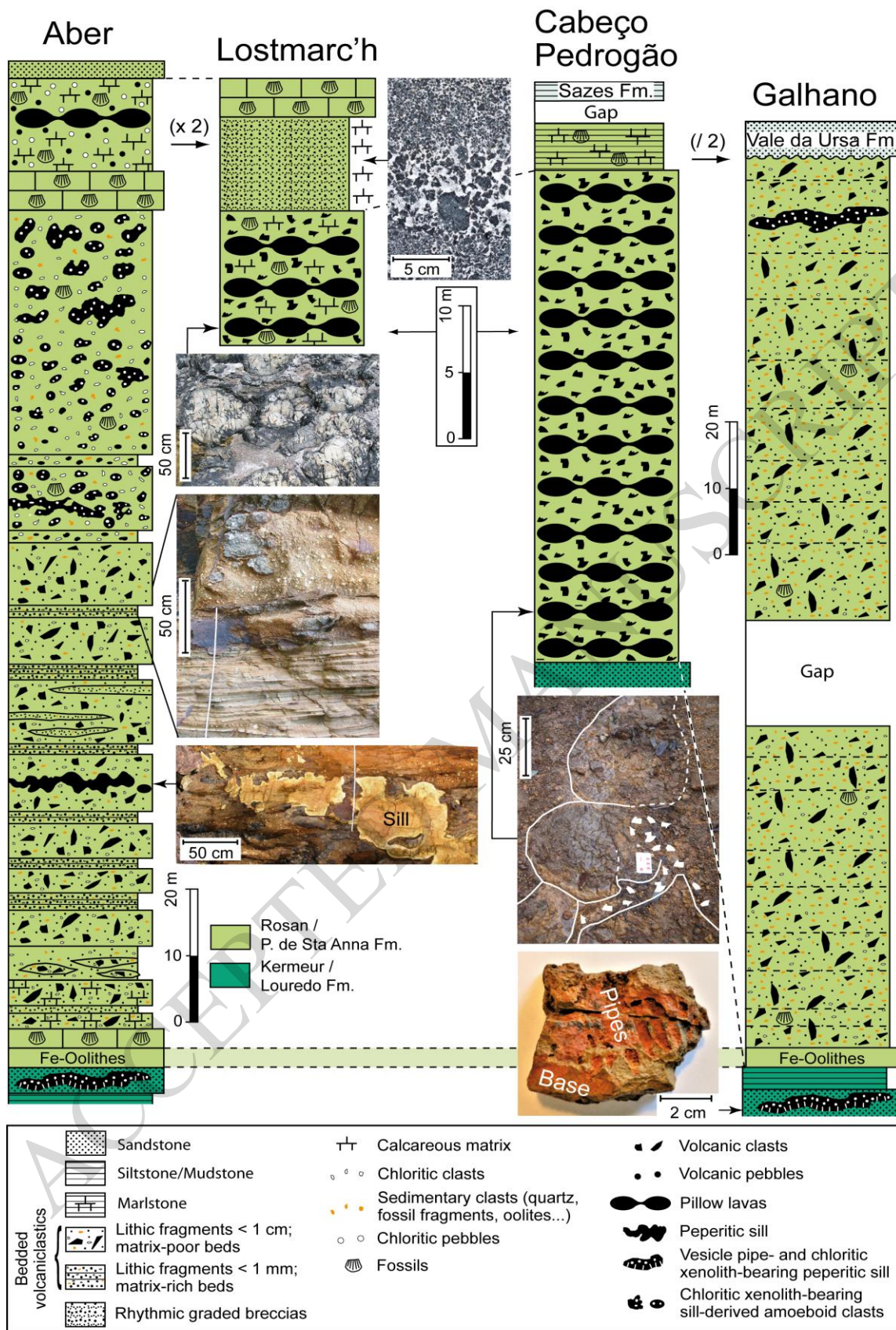
Caroff, Fig. 1



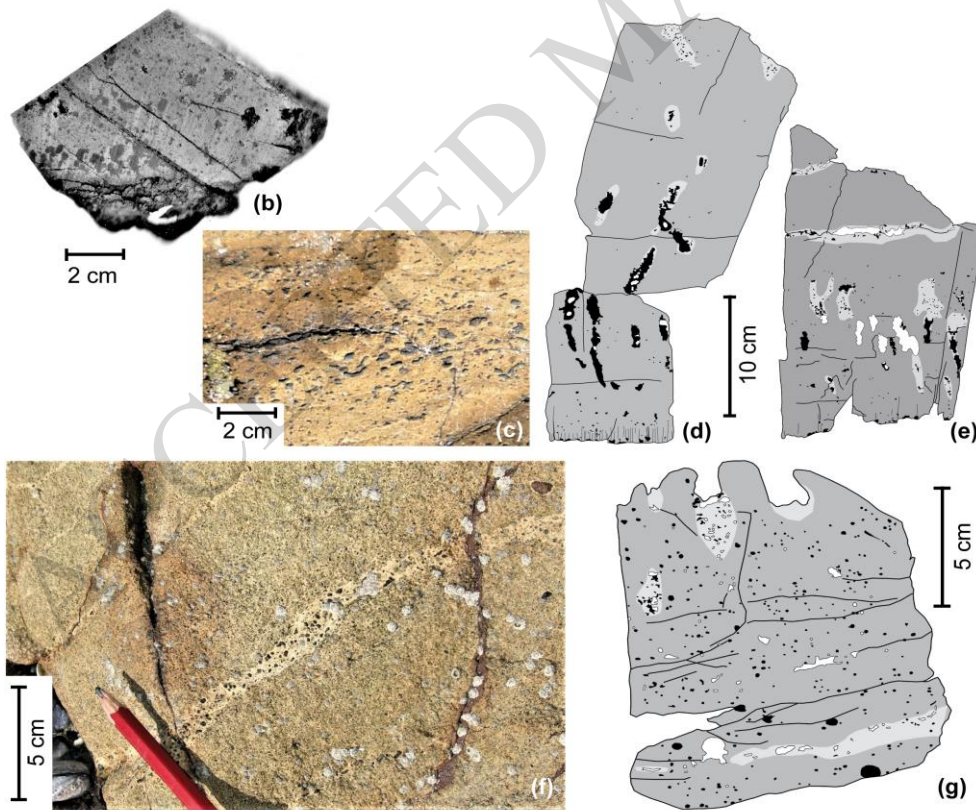
Caroff, Fig. 2



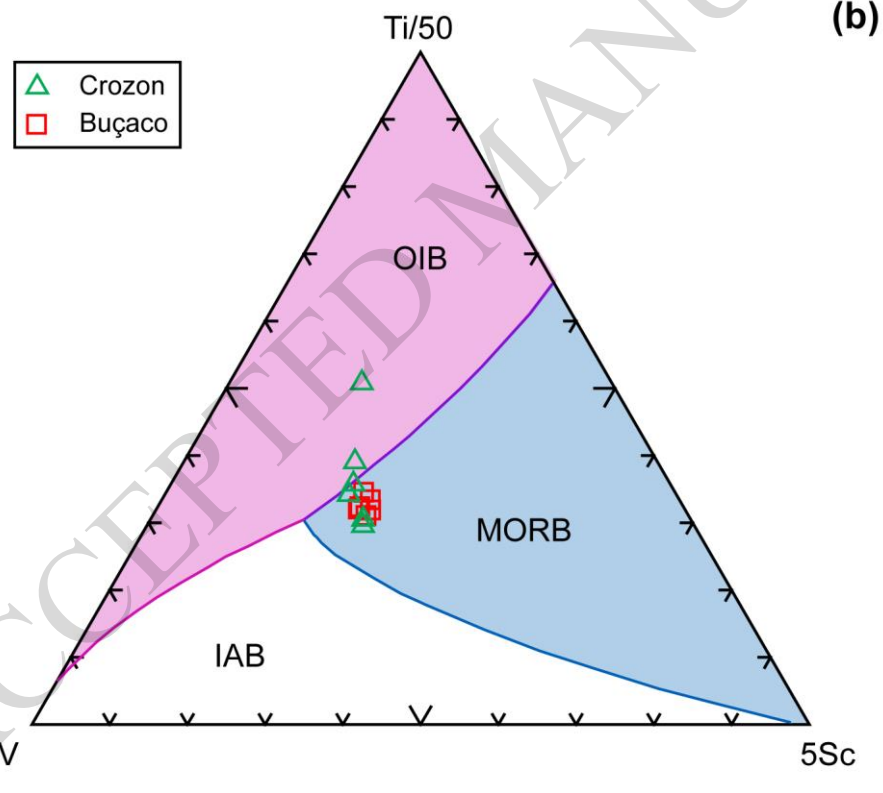
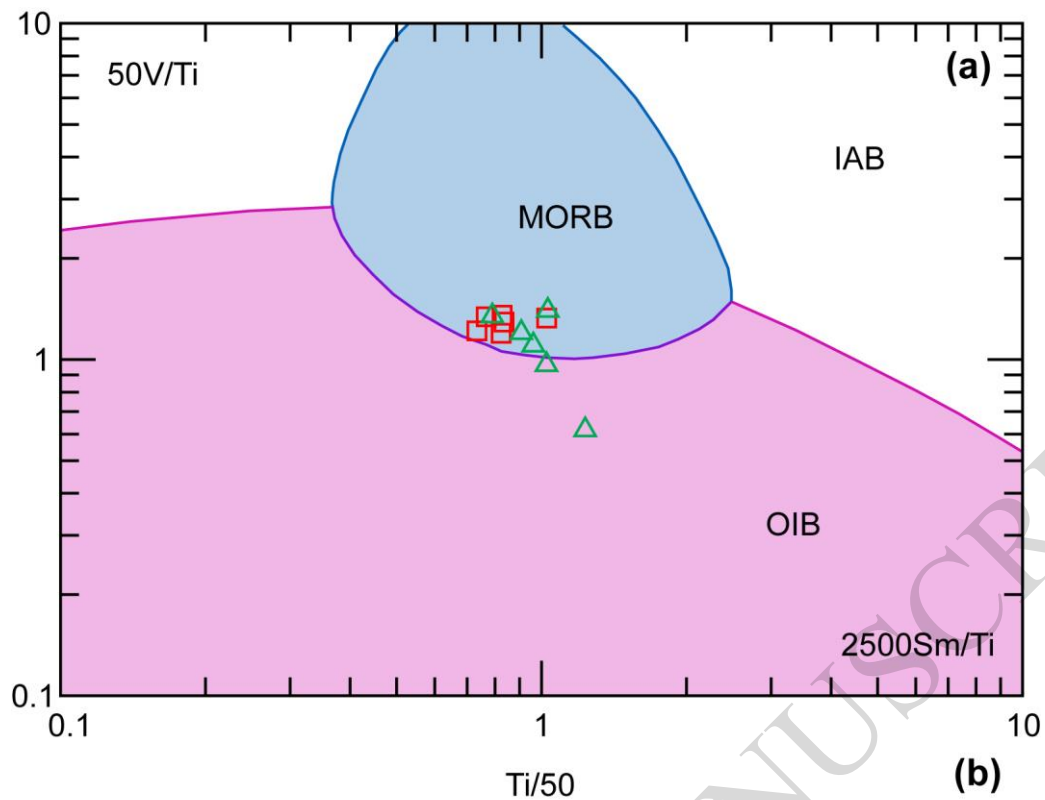
Caroff, Fig. 3



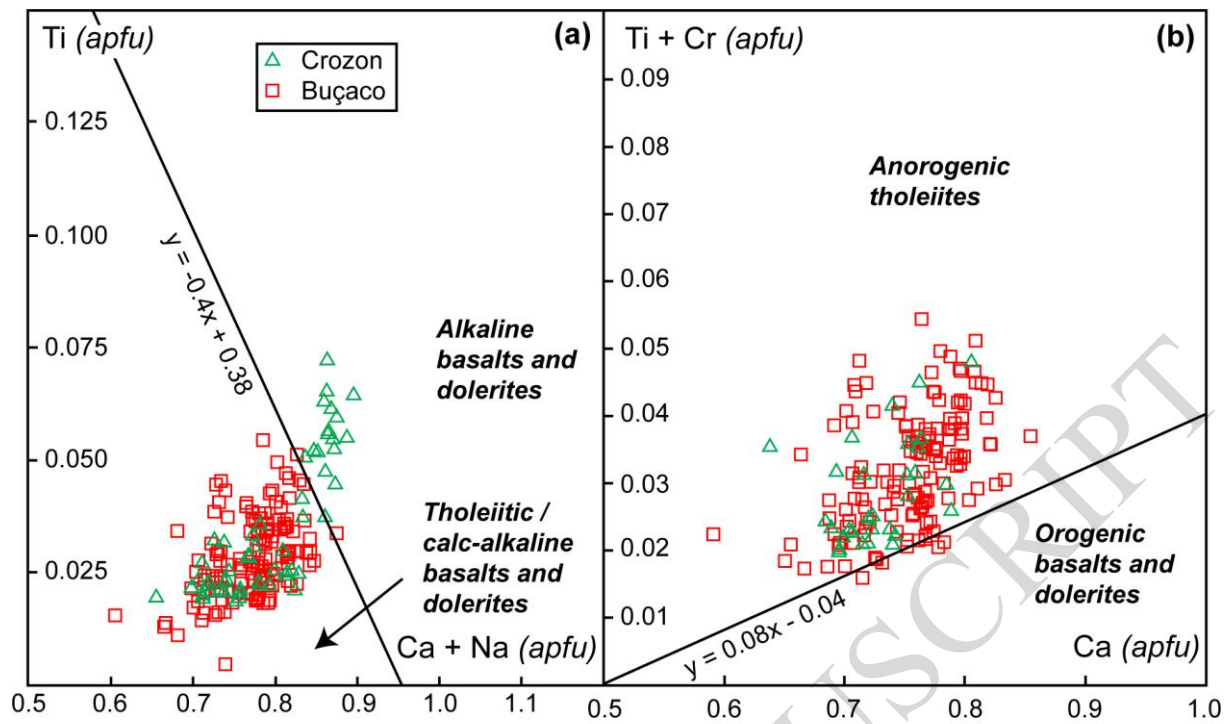
Caroff, Fig. 4



Caroff, Fig. 5

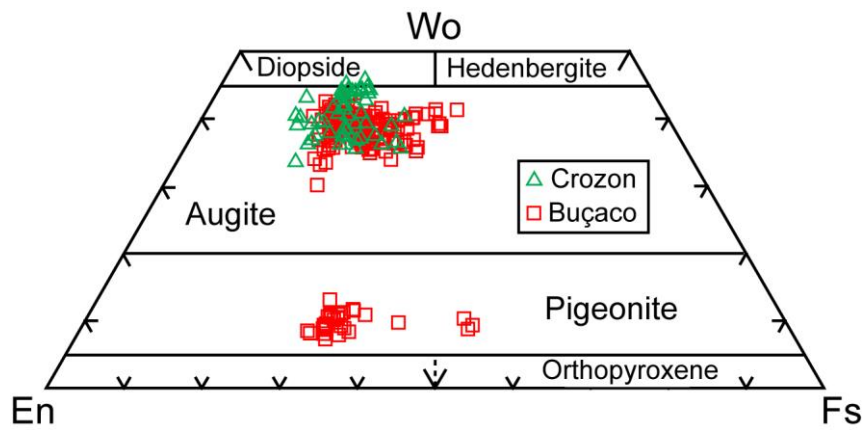


Caroff, Fig. 6



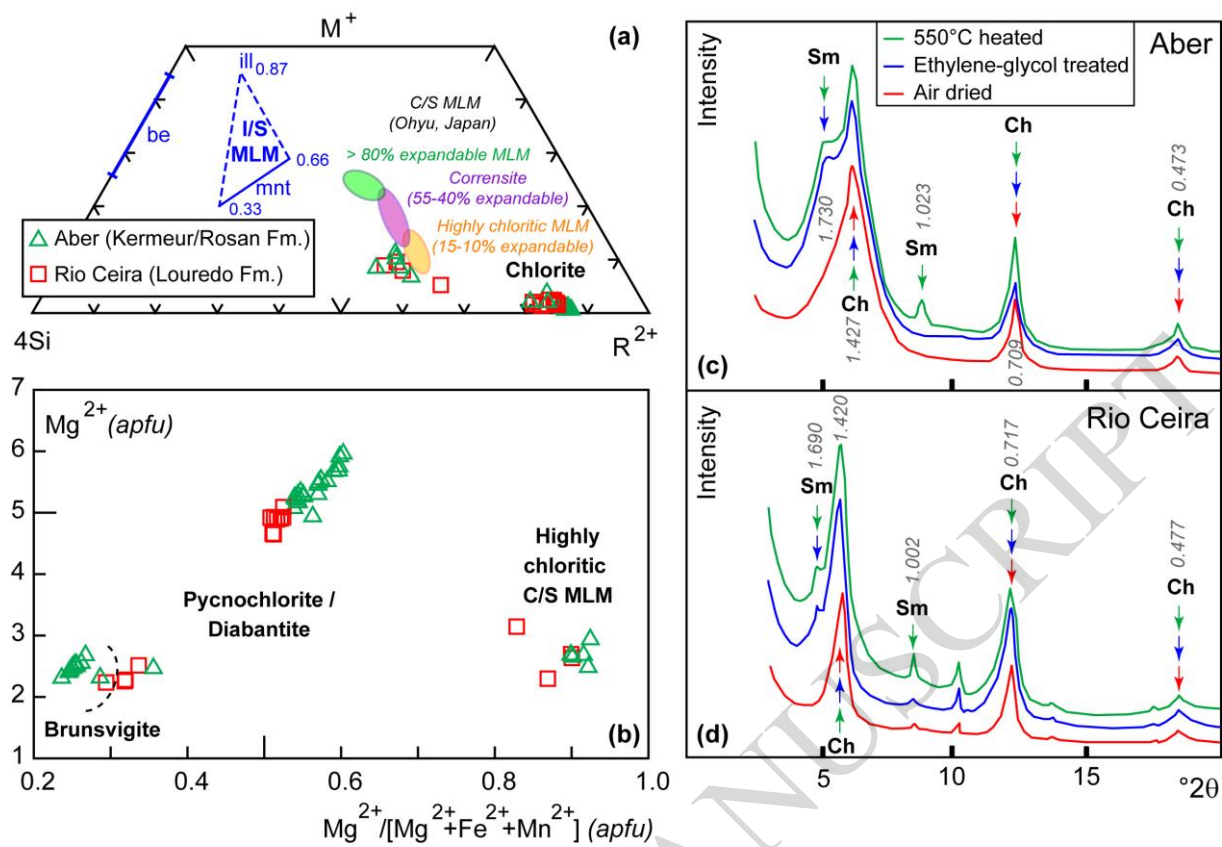
Caroff, Fig. 7

ACCEPTED MANUSCRIPT

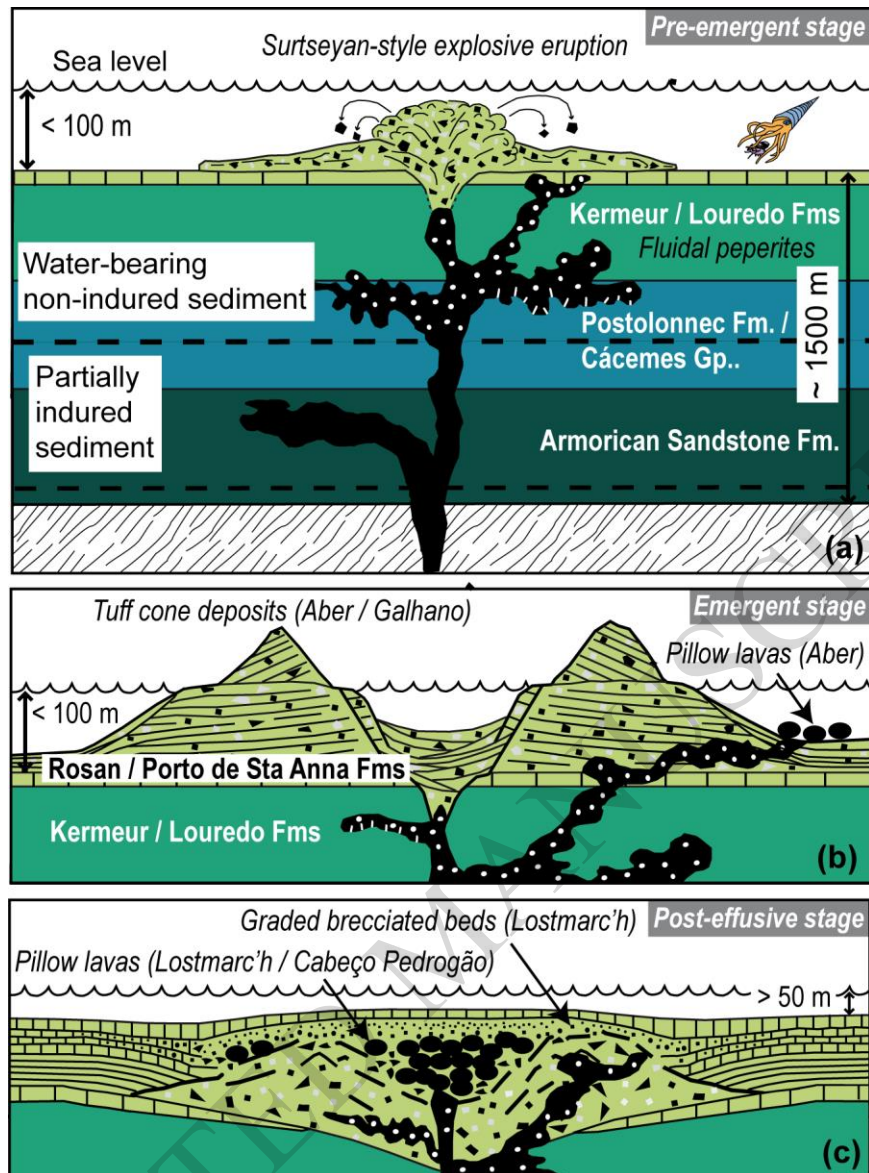


Caroff, Fig. 8

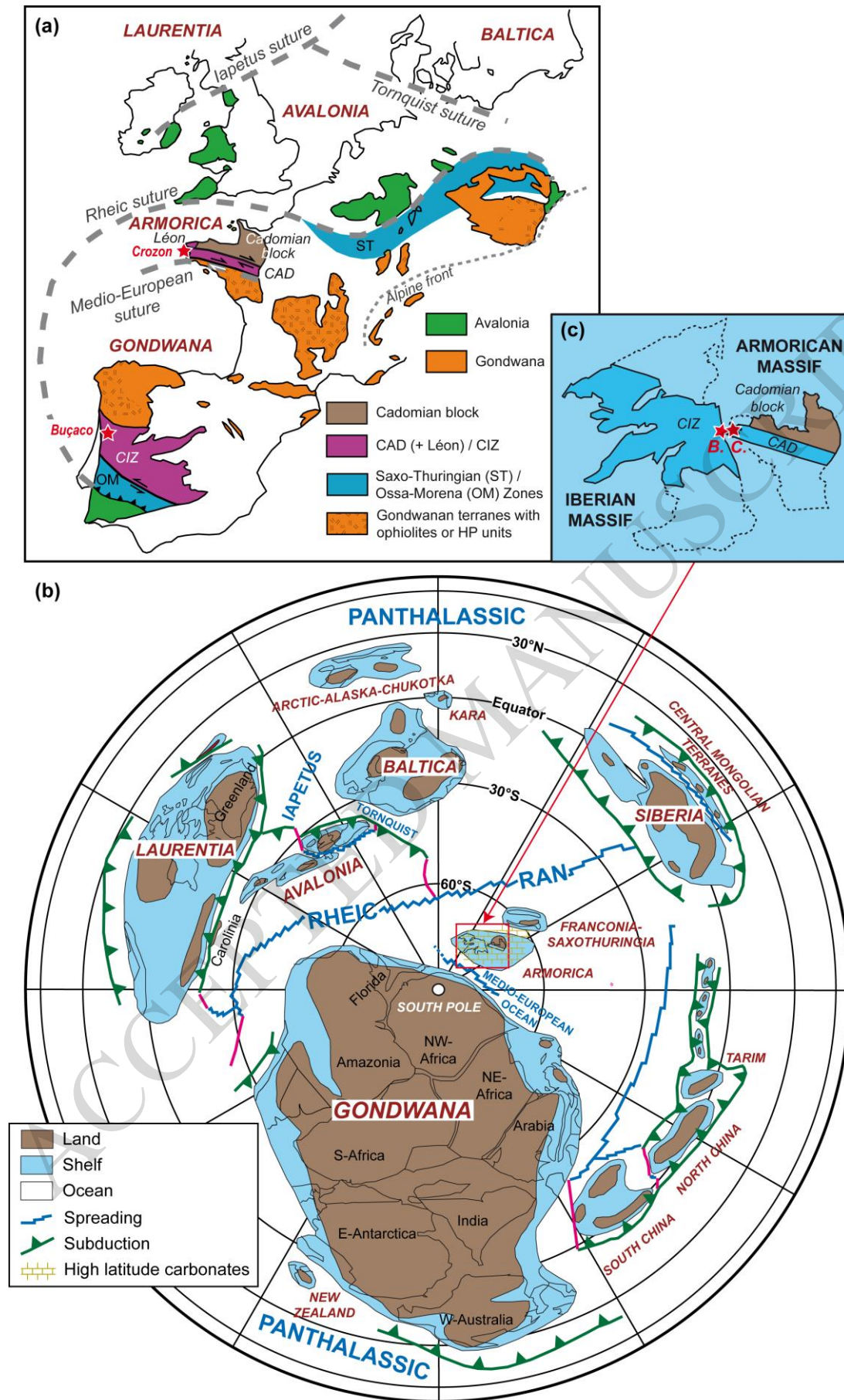
ACCEPTED MANUSCRIPT



Caroff, Fig. 9



Caroff, Fig. 10



Caroff, Fig. 11